Mantle Convection in the Earth and Planets

GERALD SCHUBERT
University of California, Los Angeles

DONALD L. TURCOTTE
Cornell University

PETER OLSON
The Johns Hopkins University

CAMBRIDGE
UNIVERSITY PRESS

PUBLISHED BY THE PRESS SYNDICATE OF THE UNIVERSITY OF CAMBRIDGE
The Pitt Building, Trumpington Street, Cambridge, United Kingdom

CAMBRIDGE UNIVERSITY PRESS
The Edinburgh Building, Cambridge CB2 2RU, UK
40 West 20th Street, New York, NY 10011-4211, USA
10 Stamford Road, Oakleigh, VIC 3166, Australia
Ruiz de Alarcón 13, 28014 Madrid, Spain
Dock House, The Waterfront, Cape Town 8001, South Africa

http://www.cambridge.org

First published 2001

Printed in the United Kingdom at the University Press, Cambridge

Typeface Times Roman 10.25/12.25 pt. *System* LaTeX2e [KW]

A catalogue record for this book is available from the British Library

Library of Congress Cataloging-in-Publication Data
Schubert, Gerald.
Mantle convection in the earth and planets/Gerald Schubert, Donald L. Turcotte, Peter Olson.
p. cm.
ISBN 0 521 35367 X hardback
ISBN 0 521 79836 1 paperback
1. Earth – Mantle. 2. Heat – Convection. 3. Geodynamics. I. Turcotte, Donald Lawson.
II. Olson, Peter. III. Title.
QE509.4.S38 2001
551.1′16 – dc2 00-058515

ISBN 0 521 35367 X hardback
ISBN 0 521 79836 1 paperback

The net contribution to the geoid anomaly comes from the negative mass anomaly at the surface induced by the internal load. The negative mass anomaly at the surface more than cancels the positive mass load at depth in contributing to the geoid anomaly. The geoid anomaly approaches zero as the load approaches the surface ($d \rightarrow 0$). The viscosity of the half-space has no effect on the geoid anomaly, which is basically why the technique discussed above for mantle viscosity determination measures only viscosity variations with depth. The viscosity in this problem determines only the relaxation time scale on which the internal load establishes the long-term surface deflection.

5.6 Incorporation of Surface Plate Motion

The two-layer viscosity structure obtained from applications of seismic tomography to the nonhydrostatic geoid is at variance with most published models of viscosity structure derived from postglacial rebound. The former approach yields a relatively high viscosity lower mantle separated at 660–1,200 km depth from a relatively low viscosity upper mantle, while the latter procedure gives a more uniform viscosity structure (see Table 5.2). In principle, additional constraints on mantle viscosity come from a consideration of horizontal forces, in particular the tractions on the base of the lithosphere that govern plate motions. It is theoretically possible to deduce the absolute viscosity of the mantle by modeling plate motions, since the velocities of plates are a result of the balance between density heterogeneity driving forces and viscous stresses resisting motion.

Several different procedures have been used to incorporate plate motion, but the basic principle behind all of them is the linear superposition of results from two viscous flow calculations, one with a rigid upper boundary condition that uses the observed distribution of subducted slabs and mantle seismic heterogeneity as the driving density heterogeneity, and another flow driven solely by the observed plate motions. By adjustment of the radial viscosity structure, solutions can be found that yield, to some approximation, zero net torque on each lithospheric plate. Ricard and Vigny (1989) and Forte et al. (1991) have explored this method and find that the coupling between plate motions and lower mantle heterogeneity is rather weak; plates are primarily driven by slabs and resisted by upper mantle viscous forces, whereas the long-wavelength geoid is mostly sensitive to lower mantle density heterogeneity and viscosity. In addition, there is a large uncertainty in the upper mantle viscosity derived from modeling plate motions, stemming from the

Table 5.2. *Two-layer Mantle Viscosity Models*

Data	Lithosphere Thickness (km)	Upper Mantle Viscosity (Pa s)	Lower Mantle Viscosity (Pa s)
Postglacial rebound[1]	120	1×10^{21}	4.5×10^{21}
Geoid[2]	100	2×10^{19}	6×10^{21}
Geoid and plate velocities[3]	100	2.6×10^{20}	1.3×10^{22}
Continental margins[4]	75	2×10^{20}	7.5×10^{21}
Ocean Islands[5]	50	1×10^{20}	1×10^{22}

[1]Mitrovica and Peltier (1991), [2]Hager and Richards (1989), [3]Ricard and Vigny (1989), [4]Lambeck and Nakada (1990), [5]Nakada and Lambeck (1989).

numerous simplifying assumptions that are invoked in order to simulate plates with a viscous fluid model. These include neglect of edge forces such as fault resistance and neglect of lateral variations in viscosity, which are especially significant near plate margins. Nevertheless, consideration of plate motions seems to constrain the upper mantle viscosity to a value near 10^{20} Pa s, in reasonable agreement with the results of postglacial rebound studies.

5.7 Application of Inverse Methods

Most studies of mantle viscosity yield viscosity structures that agree within about an order of magnitude. The principal disagreement concerns the difference in viscosity between the upper mantle and the lower mantle. A number of these studies are summarized in Table 5.2. Arguments favoring a near-uniform viscosity mantle based on deglaciation studies have been given by Tushingham and Peltier (1992), who suggest $\mu = 10^{21}$ Pa s in the upper mantle and $\mu = 2 \times 10^{21}$ Pa s in the lower mantle. Arguments favoring an order of magnitude difference in viscosity between the upper mantle and the lower mantle, also based on glaciation studies, have been given by Lambeck et al. (1990), who suggest $\mu = 3\text{–}5 \times 10^{20}$ Pa s in the upper mantle and $\mu = 2\text{–}7 \times 10^{21}$ Pa s in the lower mantle. Again, based on glaciation studies, it is concluded that the viscosity of the mantle falls in the range $0.65\text{–}1.10 \times 10^{21}$ Pa s from the base of the lithosphere to a depth of 1,400 km; Mitrovica and Peltier (1995) argue that the lower mantle viscosity is in the range $0.5\text{–}3 \times 10^{21}$ Pa s, and Peltier and Jiang (1996) suggest that the deepest part of the mantle has a factor of 10 higher viscosity than the upper part of the lower mantle. Peltier (1996a) and Lambeck and Johnston (1998) have reviewed many of these results.

Motivated by the disparities among mantle viscosity models, a number of authors have attempted to use the formalism of inverse theory to establish some reliable bounds on the class of acceptable viscosity structures. King (1995a) has organized the main results of inversions that rely primarily on data from plate motions, postglacial rebound, and the geoid. These are summarized in Figures 5.13–5.15.

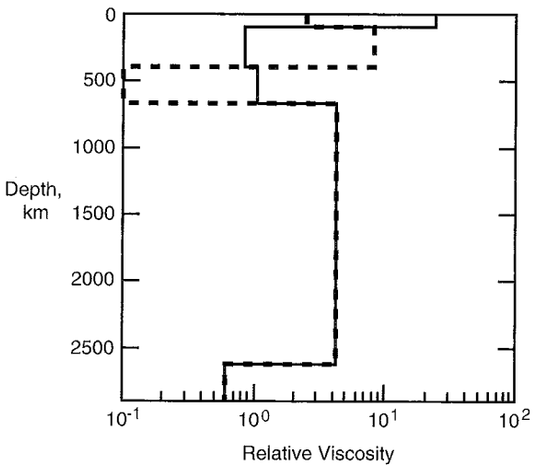

Figure 5.13. Suite of five-layer mantle viscosity profiles obtained by Forte et al. (1991) using mantle heterogeneity from seismic tomography and plate velocities. The preferred model is shown by the dashed line. The viscosity scale factor is 10^{21} Pa s.

Figure 5.13 shows viscosity profiles obtained by Forte et al. (1991) from plate motion data, using the method of Baysian inference. The profiles are based on a five-layer parameterization, and the heavy dashed line represents the preferred model. Note the presence of a low-viscosity channel at transition zone depths, as well as low-viscosity in the D″ layer. Figure 5.14 shows the result of a three-layer parameterized model obtained by Ricard et al. (1989) using Monte Carlo inversion of geoid and plate velocity data. This inversion produced two distinct classes of acceptable solutions, one with a low-viscosity transition zone, the other with high viscosity in the transition zone and relatively low-viscosity in the lower mantle. Finally, Figure 5.15 shows the results of an inversion by King and Masters (1992) using mantle S-wave velocity structure, the geoid, and an 11-layer parameterization. The examples of acceptable models are rather similar in this study, and all exhibit a low-viscosity transition zone and viscosity increases in the depth range 660–1,200 km.

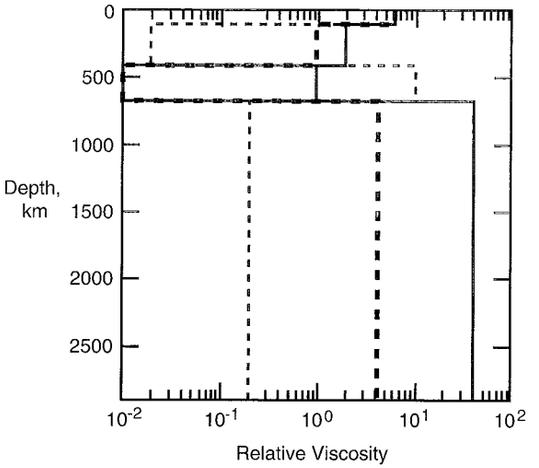

Figure 5.14. Suite of three-layer mantle viscosity profiles obtained by Ricard et al. (1989) using mantle heterogeneity from seismic tomography, plate velocities, and the geoid in a Monte Carlo inversion. The preferred model is shown by the heavy dashed line. The viscosity scale factor is 10^{21} Pa s.

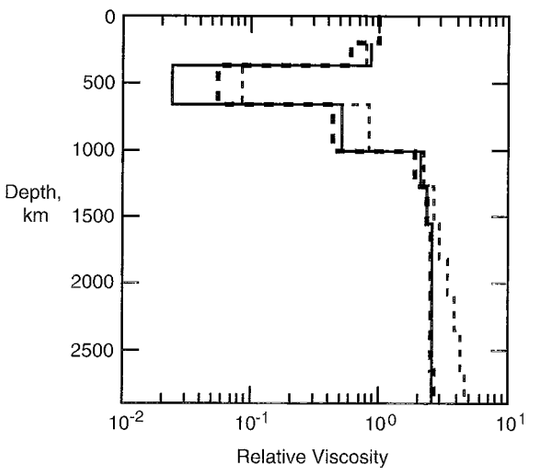

Figure 5.15. Suite of 11-layer mantle viscosity profiles obtained by King and Masters (1992) using mantle heterogeneity from S-wave tomography and the geoid. The preferred model is shown by the heavy dashed line. The viscosity scale factor is 10^{21} Pa s.

5.8 Summary of Radial Viscosity Structure

The differences among the various viscosity models in Table 5.2 and in Figures 5.13–5.15 reflect inconsistencies among the methods of inferring viscosity, lack of resolving power in the data and, in addition, the possibility of large lateral viscosity variations in the mantle. Even with these complications, it is possible to draw some general conclusions. First, the upper mantle is less viscous than the lower mantle, on average. The difference in average viscosity may only be a factor of 3, or alternatively it may be as much as 30. In either case the difference is substantial for mantle convection processes. The region where this increase occurs is at least as deep as the 660 km discontinuity and may be as deep as 1,200 km. The average viscosity of the upper mantle (beneath the lithosphere) is less than the canonical value of $\mu = 10^{21}$ Pa s, and the average viscosity for the lower mantle is higher than this value. In some regions there is unambiguous evidence for a low-viscosity asthenosphere, especially beneath the oceanic lithosphere, with viscosities in the range 10^{19}–10^{20} Pa s. In all likelihood, lateral variations in viscosity in this region are large, making global average characterizations both difficult to define and misleading to use (D'Agostino et al., 1997; Giunchi et al., 1997). There is an indication of a low-viscosity region at the base of the transition zone, although this feature awaits further delineation and confirmation. There is no compelling evidence for a huge viscosity increase through the lower mantle, as might result from a strong pressure effect.

Question 5.4: *What is the difference between the viscosity of the upper mantle and the viscosity of the lower mantle?*

5.9 Physics of Mantle Creep

At temperatures that are a substantial fraction of their melting temperatures, crystalline solids deform "slowly" like a fluid. This creep deformation occurs under an applied stress due to thermally activated motion of atoms and ions associated with crystalline defects such as dislocations and atomic vacancies. The principal deformation mechanisms associated with mantle convection are atom/ion migration (known as diffusion or Herring-Nabarro creep if the migration occurs within grains and Coble creep if it occurs along grain boundaries) and dislocation migration (dislocation creep). The applicability of these processes to the deformation of the mantle was first proposed by Gordon (1967).

We first consider diffusion creep. Vacancies are empty sites in the crystalline lattice (Figure 5.16). At any nonzero temperature there is an equilibrium concentration of vacancies that is temperature dependent. Atoms migrate by the movement of adjacent vacancies (Figure 5.17); this is basically a diffusion process and it results in deformation or creep (Figure 5.18). Diffusion of atoms in a crystalline solid is a thermally activated process. The relevant diffusion coefficient D is given by the Arrhenius relation

$$D = D_0 \exp\left[-\frac{(E^* + pV^*)}{RT}\right] \tag{5.9.1}$$

where E^* is the activation energy per mole, V^* is the activation volume per mole, R is the universal gas constant, and D_0 is the frequency factor. The activation energy is the sum of the energy of formation of a vacancy and the energy barrier preventing the migration of an

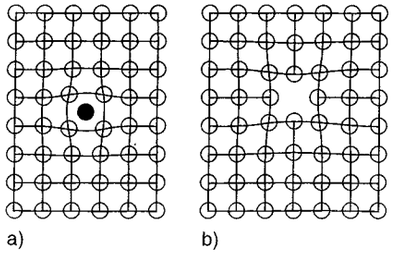

Figure 5.16. Point defects in a crystal lattice. (a) An interstitial or extra atom, (b) a vacancy. The lattice tends to distort around the defect. After Twiss and Moores (1992).

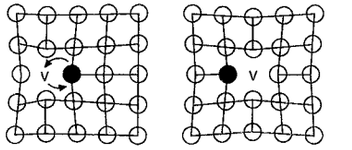

Figure 5.17. Illustration of the motion of a vacancy (v) from one lattice site to an adjacent one by the opposite motion of an atom (solid circle). Matter and vacancies diffuse in opposite directions. After Twiss and Moores (1992).

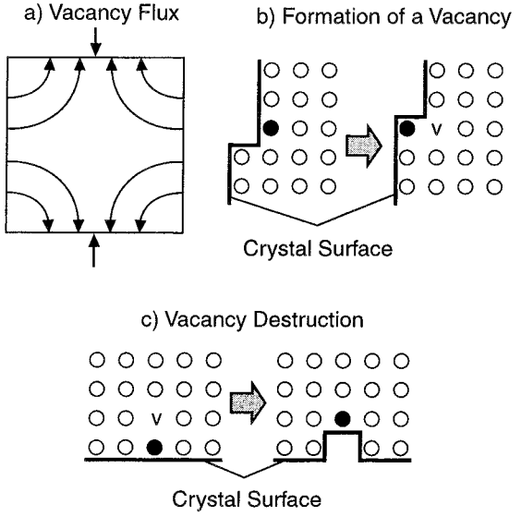

Figure 5.18. Diffusion creep or Herring-Nabarro creep due to vacancy diffusion in a crystal under uniaxial compression. (a) Vacancies diffuse toward the surface of highest normal (compressive) stress along the indicated paths. Atoms diffuse in the opposite direction. (b) Creation of a vacancy at a surface of minimum compressive stress. The solid lines mark the crystal surface. The solid circle marks the ion whose position changes to create the vacancy (v). The surface gradually builds out, lengthening the crystal normal to the compressive stress. Vacancies diffuse toward a surface of high compressive stress. (c) Destruction of a vacancy at a surface of maximum compressive stress. Removal of atoms from the surface and destruction of vacancies gradually shortens the crystal parallel to the maximum compressive stress. After Twiss and Moores (1992).

atom into an adjacent vacancy site, and the term pV^* takes account of the effect of pressure in reducing the number of vacancies and increasing the energy barrier. The exponential temperature dependence follows directly from the Maxwell–Boltzmann distribution of atomic energies. It gives the fraction of atoms that have sufficient energy to overcome the energy

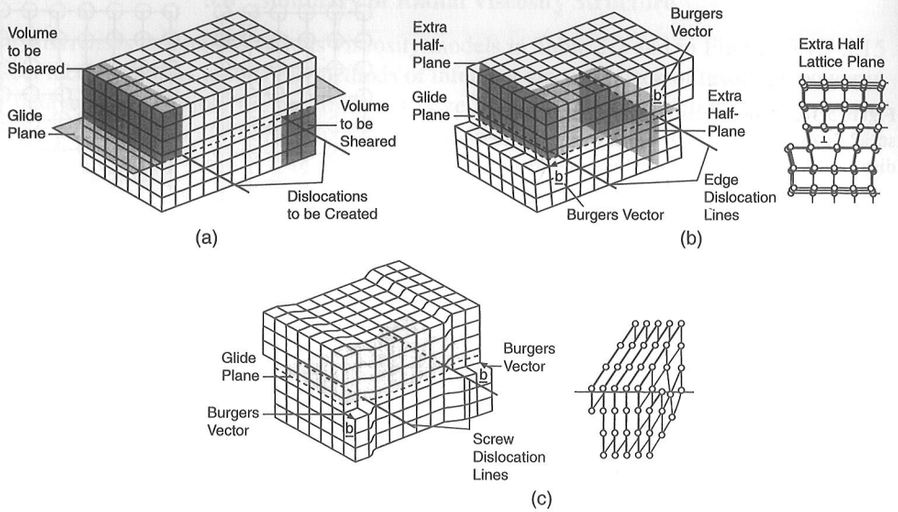

Figure 5.19. Geometry of edge and screw dislocations. The two examples of each type of dislocation in lattice blocks of (b) and (c) are dislocations of opposite sign. b is the Burgers vector. (a) A perfect crystal lattice into which dislocations are introduced in (b) and (c). (b) Edge dislocations of opposite sign produced by shearing the shaded volumes (a) in a direction perpendicular to its interior edge. Each dislocation is at the edge of an extra half-plane of lattice points. The diagram to the right is a view down the edge dislocation line. The inverted T symbol stands for an edge dislocation. (c) Screw dislocations of opposite sign produced by shearing the shaded volumes in (a) one lattice dimension in a direction parallel to its interior edge. The diagram to the right shows that the crystal lattice planes form a continuous helical surface around the dislocation line. After Twiss and Moores (1992).

barrier between lattice sites and can thus jump into a vacancy as well as the fraction of lattice sites that are vacancies. It is also possible to account for both the temperature and pressure dependences of the diffusion coefficient using the relation

$$D = D_0 \exp\left(-\frac{aT_m}{T}\right) \tag{5.9.2}$$

where T_m is the melting temperature of the crystalline solid. The ratio T/T_m is referred to as the homologous temperature. The pressure dependence of the diffusion coefficient is accounted for by the pressure dependence of the melting temperature. Diffusion coefficients in silicate minerals have been reviewed by Freer (1981).

We now turn to dislocation creep. Dislocations are line or one-dimensional imperfections in the crystalline lattice (Figure 5.19). A dislocation is defined in terms of the Burgers vector b which is a measure of the relative atomic motion (slip) that occurs when a dislocation line passes through a lattice (Figure 5.19). The surface that traces the motion of a dislocation line is the glide surface, and such surfaces are usually planar (Figure 5.19). Specification of the Burgers vector and the line direction fully defines a dislocation. If the dislocation line is parallel to the Burgers vector, it is a screw dislocation (Figure 5.19). If the dislocation line is perpendicular to the Burgers vector, it is an edge dislocation (Figure 5.19). Most dislocations have both edge and screw components (Figure 5.20).

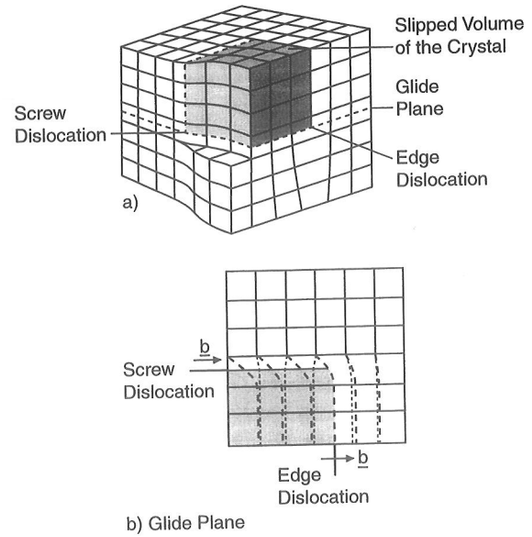

Figure 5.20. Boundaries of slipped portions of a crystal lattice. (a) The shaded volume of the crystal has slipped relative to the unshaded part. The boundaries of the glide plane are an edge and a screw dislocation. (b) View of the glide plane. The shaded area is the area over which slip has occurred. The boundary is an edge dislocation where b is normal to the boundary. The boundary is a screw dislocation where b is parallel to the boundary. Dotted and dashed lines show planes below and above the glide plane, respectively. After Twiss and Moores (1992).

The two principal ways in which dislocations can contribute to creep are by dislocation slip or glide and dislocation climb. In dislocation slip, the dislocation line moves through the lattice breaking interatomic bonds as it moves (Figure 5.21). This motion conserves mass because it does not require the addition or removal of atoms. Edge dislocations (or the edge components of mixed dislocations) also move by dislocation climb (Figure 5.22). In dislocation climb, the dislocation line moves by the addition of atoms. This is not mass conserving because it requires the diffusion of atoms from elsewhere in the lattice. Dislocation creep can also be thermally activated at relatively low stress levels. Again, the Maxwell–Boltzmann distribution gives the number of atoms that have sufficient energy to overcome the interatomic bonds restricting the motion of a dislocation.

Experiments and theory indicate that a general form of the relationship between strain rate $\dot{e}$ and deviatoric stress τ valid for both diffusion and dislocation creep is given by

$$\dot{e} = A\left(\frac{\tau}{\mu}\right)^n \left(\frac{b}{d}\right)^m \exp\left[-\frac{(E^* + pV^*)}{RT}\right] \tag{5.9.3}$$

where A is the pre-exponential factor, μ is the shear modulus, d is the grain size, and b is the magnitude of the Burgers vector. Typical values of n and m are $n = 1$ and $m = 2.5$ for diffusion creep and $n = 3.5$ and $m = 0$ for dislocation creep. For diffusion creep, the relation between strain rate $\dot{e}$ and deviatoric stress τ is linear, resulting in a Newtonian viscosity. For dislocation creep, the relation between strain rate $\dot{e}$ and deviatoric stress τ is strongly nonlinear, resulting in a nonlinear viscous rheology. Another difference between these mechanisms is the dependence on grain size. The diffusion creep viscosity decreases strongly with decreasing grain size d, while dislocation creep is insensitive to changes in grain size.

Grain boundaries are two-dimensional defects separating adjacent crystals with different lattice orientations. Grain size is controlled by grain growth and, in the dislocation creep regime, by dynamic recrystallization (De Bresser et al., 1998). Grain growth is a process that

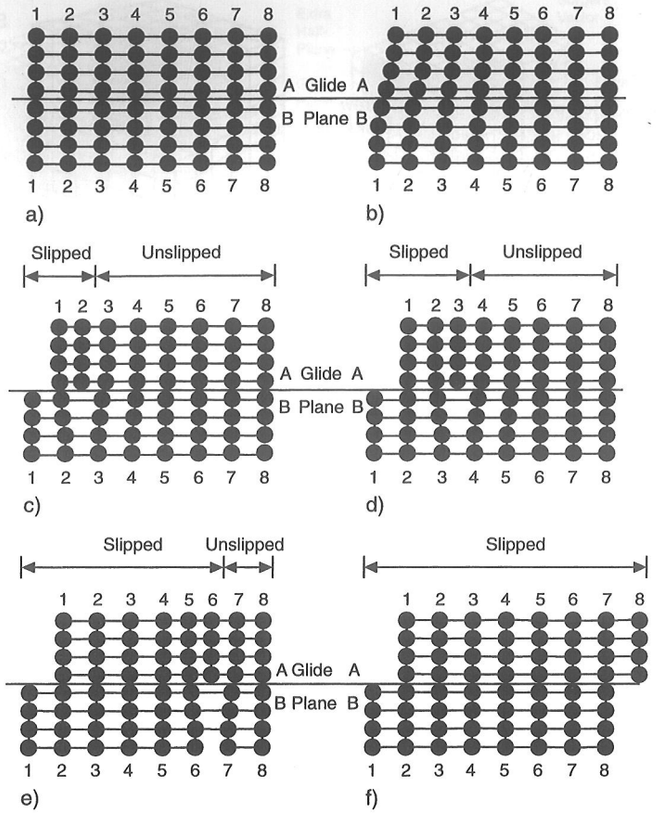

Figure 5.21. The glide or slip of a dislocation through a crystal lattice is accomplished by switching bonds of neighboring atoms across the glide plane. (a) through (f) illustrate the process of forming an edge dislocation and moving it through the crystal to produce one Burgers vector offset in the crystal. Crystallographic planes in the undeformed crystal are numbered 1 through 8. The letters A and B refer to parts of the crystal above and below the slip plane, respectively. After Twiss and Moores (1992).

reduces total energy by decreasing the grain boundary area per unit volume. Grain growth is the only process to control the size of grains in the diffusion creep regime. Clearly, grain growth would increase the size of grains with time until grain size was large enough to result in dislocation creep. However, the presence of other phases limits grain growth (Zener pinning) and stabilizes grain size. Therefore, grain size can be small and diffusion creep could be occurring in the mantle.

Creation and migration of new grain boundaries in a stressed crystal can reduce the strain energy. This is dynamic recrystallization which can occur only under dislocation creep. The higher the applied stress, the smaller the recrystallization grain size. In a monomineralic rock the steady-state grain size d in the dislocation creep regime is related to the applied deviatoric stress τ by

$$d = Kb\left(\frac{\tau}{\mu}\right)^{-q} \tag{5.9.4}$$

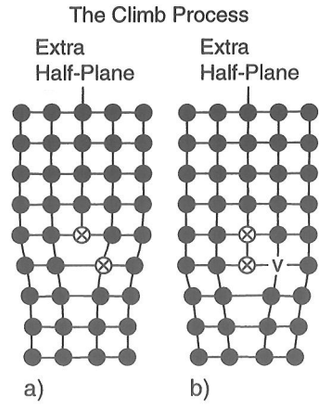

Figure 5.22. Schematic showing the climb of an edge dislocation. The dislocation climbs downward if an atom from a neighboring site jumps on to the extra half-plane (a to b) leaving a vacancy (v) behind which can then diffuse away. The dislocation climbs upward if a vacancy diffuses to a neighboring site and then jumps onto the extra half-plane (b to a). After Twiss and Moores (1992).

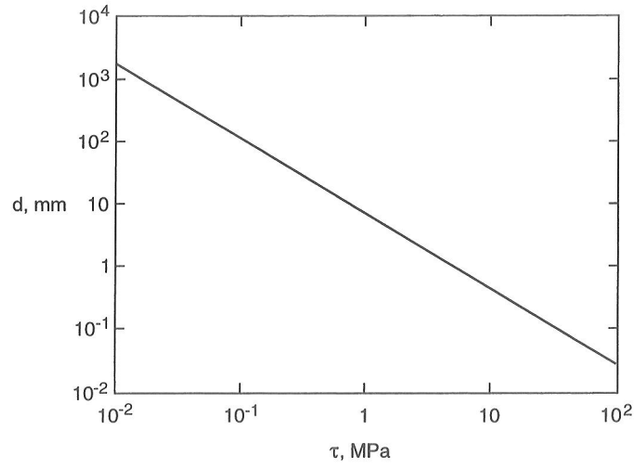

Figure 5.23. Dependence of grain size d on the deviatoric stress τ from (5.9.4).

where b is the magnitude of the Burgers vector, μ is the shear modulus, and K and q are nondimensional constants. The dependence of d on τ is given in Figure 5.23 for $K = 19$, $q = 1.2$, $b = 0.5$ nm, and $\mu = 80$ GPa, values appropriate for typical upper mantle minerals. The prediction of (5.9.4) is that grains can grow to meter size or larger with considerable reduction in deviatoric stress. This clearly cannot happen in the polycrystalline mantle of the Earth. The dependence of grain size on stress in the Earth's mantle remains controversial. Extensive discussions of creep processes applicable to mantle convection have been given by Weertman (1970), Ashby and Verrall (1977), Poirier (1985, 1995), Ranalli (1995), Evans and Kohlstedt (1995), and Drury and Fitz Gerald (1998).

Question 5.5: *What is the dependence of grain size on deviatoric stress in the mantle?*

The major minerals in the upper mantle are olivine, orthopyroxene, clinopyroxene, and garnets (see Chapter 3). One mineral can control the rheology of a rock if its volume fraction is greater than 20–30%, if it is significantly weaker than the other minerals, and if it forms an interconnected matrix. Olivine is the most abundant mineral and it is also probably the weakest, so that its rheology is likely to be dominant.

Laboratory experiments provide a direct means of determining the creep properties of mantle minerals (Goetze and Kohlstedt, 1973; Kohlstedt and Goetze, 1974). However, this approach does have serious difficulties, as noted in Section 5.1.6. In order to achieve steady-state deformation on reasonable (laboratory) time scales, the measurements must be carried out at much higher strain rates or higher temperatures than those associated with mantle convection. The laboratory results must then be extrapolated over many orders of magnitude in strain rate for application to the mantle. Also, laboratory experiments are generally carried out at much lower pressures than encountered in the mantle, again requiring a large extrapolation of results to mantle conditions.

Many laboratory measurements of olivine deformation have been carried out. These have been reviewed by Tsenn and Carter (1987), Karato and Wu (1993), Evans and Kohlstedt (1995), Kohlstedt et al. (1995), and Drury and Fitz Gerald (1998). The parameters for diffusion creep and dislocation creep in a dry upper mantle, as summarized by Karato and Wu (1993), are given in Table 5.3. An important question is whether diffusion creep is the applicable deformation mechanism in the upper mantle. The transition between dislocation creep and diffusion creep occurs when, for a given stress, the strain rates given by the two mechanisms are equal. In general, for a given stress, the deformation mechanism with the larger strain rate prevails. One way to delineate the regimes of applicability of rival deformation mechanisms is to use a deformation map (Frost and Ashby, 1982). A deformation map generally gives the stress as a function of temperature for several values of the strain rate. A deformation map for a dry upper mantle with $p = 0$, based on (5.9.3) and the parameter values in Table 5.3, is given in Figure 5.24. The diffusion creep values are based on a grain size $d = 3$ mm. This is a typical value for mantle rocks found in diatremes and in ophiolites. Dislocation creep is the applicable deformation mechanism for high stress levels and high

Table 5.3. ***Parameter Values for Diffusion Creep and Dislocation Creep in a Dry Upper Mantle***[a]

Quantity	Diffusion Creep	Dislocation Creep
Pre-exponential factor A (s^{-1})	8.7×10^{15}	3.5×10^{22}
Stress exponent n	1	3.5
Grain size exponent m	3	0
Activation energy E^* ($kJ\,mol^{-1}$)	300	540
Activation volume V^* ($m^3\,mol^{-1}$)	6×10^{-6}	2×10^{-5}

[a] After Karato and Wu (1993). Other relevant parameter values are $\mu_{\text{shear modulus}} = 80$ GPa, $b = 0.55$ nm, and $R = 8.3144\,J\,K^{-1}\,mol^{-1}$.

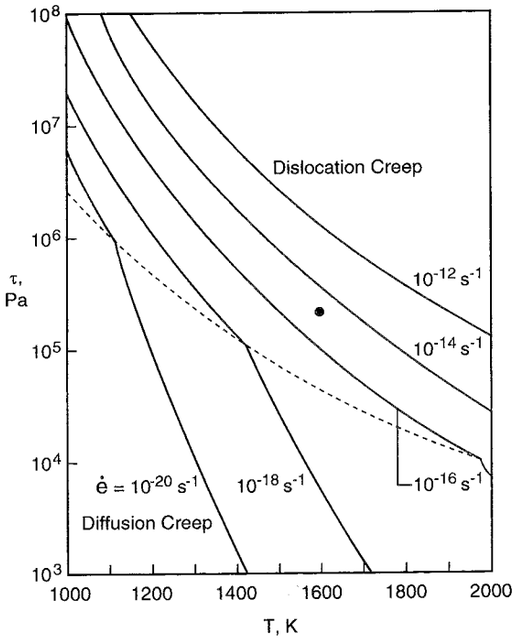

Figure 5.24. Deformation map for a dry upper mantle. The deviatoric stress τ is given as a function of temperature T for several strain rates $\dot{e}$. The dashed line separates the dislocation creep regime from the diffusion creep regime. The solid circle represents a typical condition for mantle convection.

temperatures, while diffusion creep is dominant for low stress levels and low temperatures. Uncertainties in flow law parameters lead to uncertainties of about an order of magnitude in deformation maps.

Typical values of $\dot{e}$ and T for mantle convection are $\dot{e} = 10^{-15}\,s^{-1}$ and $T = 1{,}600$ K; these values locate the large solid circle in Figure 5.24 and correspond to $\tau = 0.5$ MPa. This point clearly falls in the dislocation creep field of the upper mantle deformation map. If (5.9.4) had been used to obtain grain sizes instead of assuming $d = 3$ mm, the grain sizes would have been considerably larger and dislocation creep would have been applicable over the entire upper mantle deformation map given in Figure 5.24. Most authors who have published laboratory studies of mantle deformation have concluded that dislocation creep is the applicable deformation mechanism in the upper mantle. This conclusion is not consistent with almost all studies of postglacial rebound that favor a Newtonian viscosity for the mantle. In assessing whether dislocation creep or diffusion creep is dominant in the upper mantle, it must be emphasized that Figure 5.24 is for $p = 0$. Effects of pressure can change the dominant mechanism from dislocation creep in the shallow upper mantle to diffusion creep in the deeper upper mantle (Karato and Wu, 1993). Karato and Wu (1993) and Karato et al. (1995a) have argued that significant seismic anisotropy in the shallow upper mantle is evidence for dislocation creep at these depths, while weak seismic anisotropy in the lower mantle is evidence for diffusion creep at great depths. The nature of mantle deformation may well be a function of depth with dislocation creep occurring only in the shallow upper mantle.

Question 5.6: *Is dislocation creep or diffusion creep the dominant deformation mechanism associated with mantle convection?*

Question 5.7: *Does the mantle behave like a Newtonian or a non-Newtonian fluid on geological time scales?*

There are yet other factors contributing to our uncertainty about the viscosity of the mantle. One of these is the role of water (Hirth and Kohlstedt, 1996). Chopra and Paterson (1984) showed that trace amounts of water as low as 200–300 ppm by weight could significantly weaken olivine. Estimates of the water content of the mantle have been given by Bell and Rossman (1992). Kohlstedt et al. (1995) suggest that a dry rheology is applicable to the oceanic lithosphere and a wet rheology is applicable to the continental lithosphere. However, a high degree of depletion by melting in the continental upper mantle could mean that continental lithosphere as a whole is drier than oceanic lithosphere (Karato, 1999).

Partial melting can also influence mantle rheology (Hirth and Kohlstedt, 1995a, b; Kohlstedt and Zimmerman, 1996). Laboratory studies indicate that 1–3% melt can reduce the diffusion creep viscosity by a factor of 2–5. For dislocation creep, melt can also have a significant influence on the rheology.

The above discussion of mantle rheology has dealt mainly with the upper mantle where olivine is the principal mineral constituent. An important question is whether there will be a significant change in rheology across the 410 and 660 km seismic discontinuities. Between 410 and 660 km depth the dominant mineral will be spinel, and below 660 km depth the minerals (Mg, Fe)SiO_3 perovskite and magnesiowüstite will be dominant. This problem has been considered in some detail by Karato et al. (1995b). They suggest that there will be a small increase in viscosity at a depth of 410 km and a small decrease in viscosity at a depth of 660 km. Below 660 km depth the viscosity is predicted to increase with depth (pressure) so that the average lower mantle viscosity would be one to two orders of magnitude greater than the average upper mantle viscosity. The rheology of the lower mantle has been reviewed by Karato (1997).

Question 5.8: *Are there changes in viscosity associated with the solid–solid phase changes in the transition zone?*

5.10 Viscosity Functions

The scalar relationship between strain rate $\dot{e}$ and deviatoric stress τ given in (5.9.3) can be generalized to a full constitutive relation between the strain rate and deviatoric stress tensors. The generalized strain rate–deviatoric stress relation is (Christensen, 1989a)

$$\dot{e}_{ij} = \frac{1}{B}\left(\frac{\tau_2}{\mu}\right)^{n-1} \exp\left[-\left(\frac{E^* + pV^*}{RT}\right)\right]\tau_{ij} \tag{5.10.1}$$

$$B = \left(\frac{A}{\mu}\right)^{-1}\left(\frac{b}{d}\right)^{-m} \tag{5.10.2}$$

where τ_2 is the square root of the second invariant of the deviatoric stress tensor, and the coefficient B includes dependence on both rigidity and grain size. From (5.10.1) and the relation

$$\dot{e}_{ij} = \frac{1}{2\mu}\tau_{ij} \tag{5.10.3}$$

where μ is viscosity, we can identify the viscosity function as

$$\mu = \frac{B}{2}\left(\frac{\tau_2}{\mu_{\substack{\text{shear}\\\text{modulus}}}}\right)^{1-n} \exp\left\{\frac{E^* + pV^*}{RT}\right\} \tag{5.10.4}$$

On the right side of (5.10.4) we have written $\mu_{\substack{\text{shear}\\\text{modulus}}}$ for the shear modulus to avoid confusion with the viscosity function μ. For diffusion creep with $n = 1$, (5.10.4) becomes

$$\mu_{\substack{\text{diff}\\\text{creep}}} = \frac{1}{2}B_{\substack{\text{diff}\\\text{creep}}} \exp\left[\frac{\left(E^*_{\substack{\text{diff}\\\text{creep}}} + pV^*_{\substack{\text{diff}\\\text{creep}}}\right)}{RT}\right] \tag{5.10.5}$$

For a grain size $d = 3$ mm and $\mu_{\substack{\text{shear}\\\text{modulus}}} = 80$ GPa we have, from (5.9.3) and Table 5.3, $B_{\substack{\text{diff}\\\text{creep}}} = 8.1 \times 10^{11}$ Pa s. For dislocation creep with $n = 3.5$ the viscosity function is given by

$$\mu_{\substack{\text{disloc}\\\text{creep}}} = \frac{1}{2}B_{\substack{\text{disloc}\\\text{creep}}}\left(\frac{\mu_{\substack{\text{shear}\\\text{modulus}}}}{\tau_2}\right)^{2.5} \exp\left[\frac{\left(E^*_{\substack{\text{disloc}\\\text{creep}}} + pV^*_{\substack{\text{disloc}\\\text{creep}}}\right)}{RT}\right] \tag{5.10.6}$$

With $\mu_{\substack{\text{shear}\\\text{modulus}}} = 80$ GPa we have, from (5.9.3) and Table 5.3, $B_{\substack{\text{disloc}\\\text{creep}}} = 2.29 \times 10^{-12}$ Pa s. Figure 5.25 shows the dependence of the viscosity functions on temperature for shallow upper mantle conditions ($p = 0$) from (5.10.5) and (5.10.6) with parameter values given in Table 5.3. The result for diffusion creep (solid line) is independent of stress, and results for dislocation creep (dashed lines) are given for $\tau = 10^5$ and 10^6 Pa. For $\tau = 10^6$ Pa deformation is due to dislocation creep for the entire range of temperatures considered. For $\tau = 10^5$ Pa deformation is due to dislocation creep for $T > 1{,}415$ K and to diffusion creep for $T < 1{,}415$ K. For $\tau = 10^4$ Pa deformation is due to diffusion creep for the entire range of temperatures considered. Typical upper mantle viscosity and temperature values are $\mu = 3 \times 10^{20}$ Pa s and $T = 1{,}600$ K; this condition (large filled circle in Figure 5.25) lies in the dislocation creep field with $\tau = 10^5$ Pa.

It is generally concluded that laboratory studies favor dislocation creep as the dominant deformation mechanism for the shallow upper mantle. If dislocation creep also characterized the entire mantle, it would imply a strongly nonlinear rheology for the mantle with $\mu \sim \tau^{-2.5}$ as shown in (5.10.4). However, studies of mantle rheology based on postglacial rebound show that the adjustment of the mantle to shifts in surface loads is adequately described by a linear Newtonian behavior. A rationalization of these conclusions is possible if the flow associated with postglacial rebound is superimposed on a convecting mantle. If the deviatoric stresses associated with rebound are less than the deviatoric stresses associated with mantle convection, a linear behavior would be expected for rebound even in a non-Newtonian mantle (Weertman and Weertman, 1975; Wu, 1995). Another interpretation is

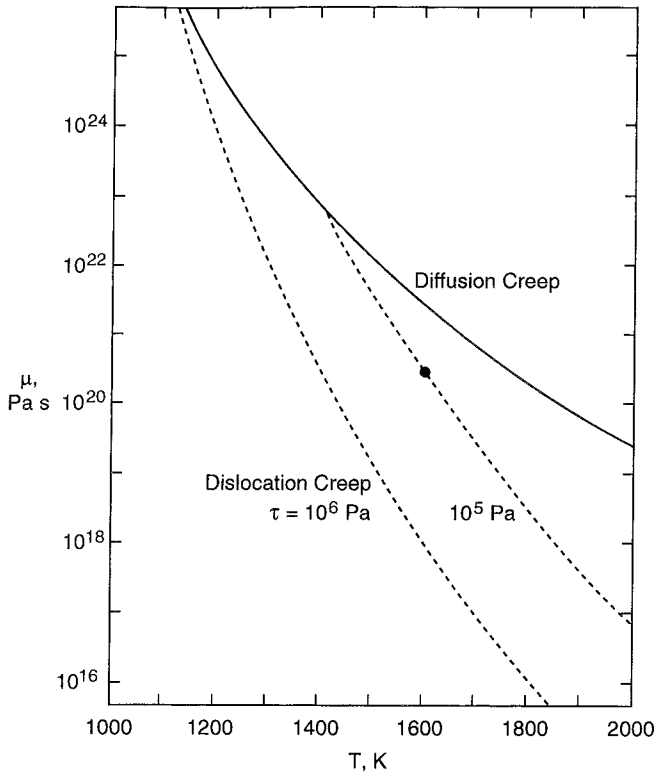

Figure 5.25. The dependence of the viscosity of a dry upper mantle on temperature is given for several stress levels. The solid line is for diffusion creep; the viscosity is not dependent on stress level. The dashed lines are for dislocation creep illustrating the dependence on the stress level. The solid circle represents a typical condition for mantle convection.

that diffusion creep characterizes all of the mantle except its shallowest depths and much of the deformation causing postglacial rebound indeed occurs in the linear Newtonian regime.

In the upper mantle, temperature variations control the behavior of the viscosity function (5.10.4), while in the lower mantle it is likely that pressure variations are equally important. Since temperature increases rapidly with increasing depth through the lithosphere, the effective viscosity drops rapidly from very high values through the lithosphere, reaching the observationally constrained range of 10^{19-21} Pa s in the asthenosphere. In the lower mantle, the influence of increasing temperature and increasing pressure act in opposite directions, so the inference of either a uniform viscosity throughout most of the lower mantle or a viscosity increasing with depth in the lower mantle is reasonable from a mineral physics perspective, although neither behavior is required.

The complete viscosity formula (5.10.4) is cumbersome to use in numerical modeling and accordingly it is often simplified. One common simplification, the exponential dependence of viscosity on temperature

$$\mu = \mu_0 \exp(-\gamma T) \tag{5.10.7}$$

is an adequate approximation over restricted temperature intervals, and it is used in applications where the pressure dependence can be neglected.